Effects of magnetic field on the perturbation between the B 1Π and c 3Σ+ states of NaK

Masaaki Baba, Kiyoshi Nishizawa, Naoki Yoshie, Kiyoshi Ishikawa, and Hajime Katô

Citation: The Journal of Chemical Physics **96**, 955 (1992); doi: 10.1063/1.462115
View online: http://dx.doi.org/10.1063/1.462115
View Table of Contents: http://scitation.aip.org/content/aip/journal/jcp/96/2?ver=pdfcov
Published by the AIP Publishing

Effects of magnetic field on the perturbation between the $B\,^1\Pi$ and $c\,^3\Sigma^+$ states of NaK

Masaaki Baba,[a] Kiyoshi Nishizawa, Naoki Yoshie, Kiyoshi Ishikawa, and Hajime Katô
Department of Chemistry, Faculty of Science, Kobe University, Nada-ku, Kobe 657, Japan

(Received 15 August 1991; accepted 1 October 1991)

Zeeman spectra of the strongly perturbed lines between the $B\,^1\Pi$ and $c\,^3\Sigma^+$ states of NaK were measured by the Doppler-free laser polarization spectroscopy. Magnetic field dependence of the Zeeman pattern was studied and the line shapes were found to change remarkably because of the mixing of the $B\,^1\Pi$ and $c\,^3\Sigma^+$ states. The patterns of Zeeman splitting were found to be different depending on whether the level was located on the high energy side or the low energy side of the interacting level. The observed Zeeman spectra were studied by taking account of the spin–orbit, hyperfine, and Zeeman interactions. The Zeeman spectroscopy is shown to be useful to analyze the perturbation between the excited states.

I. INTRODUCTION

Zeeman spectra give direct information about the magnetic properties of a molecule. Doppler-free, high-resolution laser spectroscopy made it easy to observe the Zeeman splittings,[1,2] which were usually very small and incompletely resolved by the use of a monochromator. The Zeeman spectroscopy is expected to be useful for studying the perturbation between states of different spin multiplicities. The $B\,^1\Pi$–$X\,^1\Sigma^+$ band of NaK has been studied in detail and the $B\,^1\Pi$ state is known to be strongly perturbed by the nearby $c\,^3\Sigma^+$ state in a wide energy region.[3–9] With the technique of Doppler-free laser polarization spectroscopy,[10–12] we have measured the Zeeman spectra of the strongly perturbed lines. Remarkable variations of the line splittings and intensities with the magnetic field strength were observed. We shall report the observed results and the theoretical analysis.

II. EXPERIMENT

Experimental details of the laser polarization spectroscopy have been described elsewhere.[13] We used a single-mode ring dye laser equipped with an autoscan system (Coherent CR699-29, bandwidth 500 kHz) as a light source. The output was split into the strong pump beam and the weak probe beam (10:1). They were propagated in the opposite directions and crossed in a heatpipe oven which was set at the center of an electromagnet. The pole pieces of the magnet were tapered to 50 mm diameter and the pole spacing was set to 50 mm. The magnetic field was applied perpendicular to the counterpropagating laser beams. The electric vector of a linearly polarized pump beam was set parallel to the magnetic field (π pump). A linearly polarized probe beam, whose polarization was inclined by 45° from the one of pump beam, was detected by a photomultiplier (Hamamatsu R712) through a crossed polarizer. If the laser frequency coincides with the center of the absorption, only the molecule which has no velocity component in the direction of the laser propagation can absorb both of the pump and probe beams. Then, the polarization of the probe beam is rotated slightly by an anisotropic saturation and it passes through the crossed polarizer to give rise to the signal. By modulating the pump beam by a chopper (3 kHz), the Doppler-free, high-resolution spectrum can be obtained using a lock-in amplifier (EG&G PAR model 5210). In this arrangement, only Q lines are observed with strong intensity. The laser frequency was calibrated by the fluorescence excitation spectrum of iodine and the fringe pattern of a confocal etalon [free spectral range (FSR) = 150 MHz]. The heatpipe with Na ($1g$) and K ($2g$) metals and Ar gas (0.5 Torr) was operated at 550 K. The linewidths of the rotational lines of NaK were about 40 MHz under this condition.

III. RESULTS AND DISCUSSION

Many irregularities of the rovibrational level energies were observed in the $B\,^1\Pi$ state of NaK and the hyperfine structure composed of four lines was observed in the strongly perturbed Q lines.[3–9] It was shown to originate from the mixing of the $c\,^3\Sigma^+$ state, which was found to have a large hyperfine splitting due to the Fermi contact interaction.[8,9] In addition to the energy shift and the intensity anomaly, the magnitude of hyperfine splitting of the perturbed Q line gives us information on the magnitude of mixing of the $B\,^1\Pi$ and $c\,^3\Sigma^+$ states. The Zeeman splittings of the $^1\Pi$ and $^3\Sigma^+$ states are different and the Zeeman spectra are expected to give us additional information on the singlet–triplet mixing.

The absorption coefficients α^π and α^σ for linear polarizations, respectively, parallel (π) and perpendicular (σ) to the magnetic field depend on M, which is the component of total angular momentum $\mathbf{J}$ in the field direction. For a Q branch of the $^1\Pi(J'M') \leftarrow {}^1\Sigma^+(JM)$ transition, the nonvanishing components are given by[14]

$$\alpha^\pi(JM - JM) = \mu_\perp^2 M^2/J(J+1),$$
$$\alpha^\sigma(JM \pm 1 - JM) = \mu_\perp^2 (J \pm M + 1)(J \mp M)/4J(J+1), \quad (1)$$

where $\mu_\perp$ is the electric transition dipole moment perpendicular to the molecular axis. The line strength of the laser polarization spectroscopy is proportional to $\alpha^\pi(\alpha^\pi - \alpha^\sigma)$ in the present experimental geometry. The $JM \leftarrow JM$ transition

[a] Present address: College of Liberal Arts and Sciences, Kyoto University, Sakyo-ku Kyoto 606, Japan.

has the nonvanishing value

$$\alpha^{\pi}(JM-JM)\,[\alpha^{\pi}(JM-JM)-\alpha^{\sigma}(JM-JM)] = \mu_{\perp}^4 M^4/J^2(J+1)^2. \quad (2)$$

The Zeeman splitting between the $^1\Sigma^+(JM)$ and $^1\Sigma^+(JM\pm1)$ levels at $H=10$ kG is much smaller than the natural linewidth and it can be neglected. When the Zeeman splitting between the $^1\Pi(JM)$ and $^1\Pi(JM\pm1)$ levels is smaller than the Doppler width, the cross-over signals originating from $JM\pm1 \leftarrow JM$ transitions are overlapped and the values of $\alpha^{\pi}(\alpha^{\pi}-\alpha^{\sigma})$ are given by

$$\alpha^{\pi}(JM-JM)\,[\alpha^{\pi}(JM\pm1-JM)-\alpha^{\sigma}(JM\pm1-JM)] = -\mu_{\perp}^4 M^2(J\pm M+1)(J\mp M)/4J^2(J+1)^2. \quad (3)$$

The M dependence of the $\alpha^{\pi}(JM-JM)\,[\alpha^{\pi}(JM-JM)-\alpha^{\sigma}(JM-JM)]$ and $\alpha^{\pi}(JM-JM)\,[\alpha^{\pi}(JM\pm1-JM)-\alpha^{\sigma}(JM\pm1-JM)]$ values are plotted in Fig. 1(a). The intensity of the Q line measured by the present optical arrangement is proportional to

$$\alpha^{\pi}(JM-JM)\,[\alpha^{\pi}(JM-JM)-\alpha^{\sigma}(JM-JM)] + \alpha^{\pi}(JM-JM)\,[\alpha^{\pi}(JM+1-JM)-\alpha^{\sigma}(JM+1-JM)] + \alpha^{\pi}(JM-JM)\,[\alpha^{\pi}(JM-1-JM)-\alpha^{\sigma}(JM-1-JM)]. \quad (4)$$

The M dependence is plotted in Fig. 1(b). The main contribution comes from the first term and the intensity of the laser polarization spectrum is approximately proportional to M^4.

The spectra in the range of 17 302.45–17303.05 cm^{-1} at the magnetic fields $H=0$, 1.2, and 1.8 kG are shown in Fig.

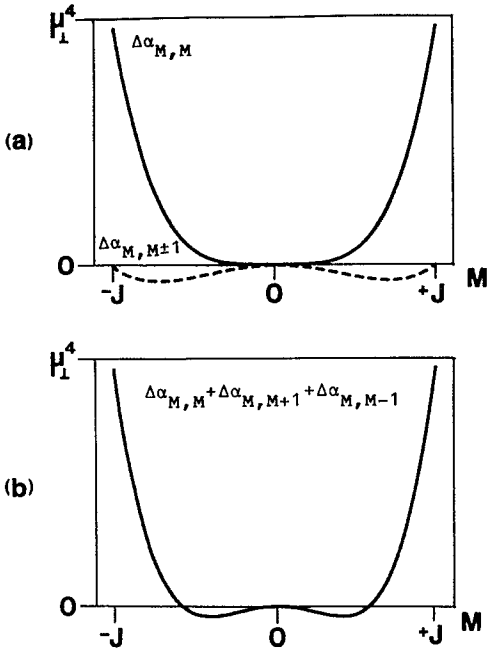

FIG. 1. M dependence of the $\Delta\alpha_{M,M'}=\alpha^{\pi}(JM-JM)\times[\alpha^{\pi}(JM'-JM)-\alpha^{\sigma}(JM'-JM)]$ values for $J=50$ is shown in (a); the full line is for $M'=M$ and the broken line is for $M'=M\pm1$. M dependence of the sum $\Delta\alpha_{M,M}+\Delta\alpha_{M,M+1}+\Delta\alpha_{M,M-1}$ is shown in (b).

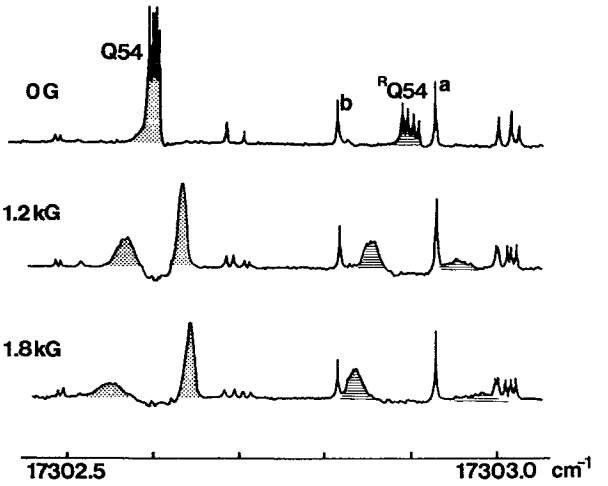

FIG. 2. Magnetic field dependence of the laser polarization spectra in the range of 17 302.45–17 303.05 cm^{-1}. Lines of the $B\,^1\Pi(v'=7, J=54f)$–$X\,^1\Sigma^+(v''=0, J=54)$ and $c\,^3\Sigma^+(v=22, N=55, F_3)$–$X\,^1\Sigma^+(v''=0, J=54)$ transitions are denoted, respectively, as $Q\,54$ and $^RQ\,54$. Both lines are shaded in the figure to distinguish from other transitions. a and b are, respectively, the lines of the $B\,^1\Pi(v'=8, J=68\ e)$–$X\,^1\Sigma^+(v''=0, J=67)$ and $B\,^1\Pi(v'=10, J=78\ e)$–$X\,^1\Sigma^+(v''=0, J=79)$ transitions.

2. The perturbation between the $B\,^1\Pi$ and $c\,^3\Sigma^+$ states is induced by the spin–orbit interaction H_{SO}. The nonvanishing matrix elements of H_{SO} between the $^1\Pi$ and $^3\Sigma^+$ levels are[9]

$$\langle {}^1\Pi v'JMf|H_{SO}|{}^3\Sigma^+ vN=J+1JM\rangle = [J/(2J+1)]^{1/2}\xi,$$
$$\langle {}^1\Pi v'JMe|H_{SO}|{}^3\Sigma^+ vN=JJM\rangle = \xi,$$
$$\langle {}^1\Pi v'JMf|H_{SO}|{}^3\Sigma^+ vN=J-1JM\rangle = [(J+1)/(2J+1)]^{1/2}\xi. \quad (5)$$

An f level of $^1\Pi(v',J)$, which can be excited by a Q line, interacts with the $^3\Sigma^+(v,N=J+1,J)$ and $^3\Sigma^+(v,N=J-1,J)$ levels through the spin–orbit interaction. The term energy (TE) of the $B\,^1\Pi(v',J)$ level in the absence of the spin–orbit interaction is calculated from the molecular constants in Ref. 9, which were derived from the unperturbed levels. The perturbed term energies (PTE) of the $B\,^1\Pi(v'=7, J=52$–$55)$ and $c\,^3\Sigma^+(v=22, N=52$–$56)$ levels are calculated from the observed transition energies and the molecular constants[15] of the $X\,^1\Sigma^+$ state. The results are shown schematically in Fig. 3. The $B\,^1\Pi(v'=7, J=54f)$ level is shifted toward low energy and the $c\,^3\Sigma^+(v=22, N=55, J=54)$ level is shifted toward high energy. This originates from the fact that the term energy (TE) of the $c\,^3\Sigma^+(v=22, N=55, J=54)$ level is at higher energy than the $B\,^1\Pi(v'=7, J=54f)$ level. Two lines of large hyperfine splitting in Fig. 2 are assigned as the $B\,^1\Pi(v'=7, J=54f)$–$X\,^1\Sigma^+(v''=0, J=54)$; $Q\,54$ and $c\,^3\Sigma^+(v=22, N=55, J=54)$–$X\,^1\Sigma^+(v''=0, J=54)$; $^RQ\,54$ transitions. The transition to a level of mainly the $B\,^1\Pi$ state character is observed with high intensity and small hyperfine splitting, whereas the transition to a level of mainly the $c\,^3\Sigma^+$ state character is observed with low intensity and large hyperfine splitting. From the difference between the

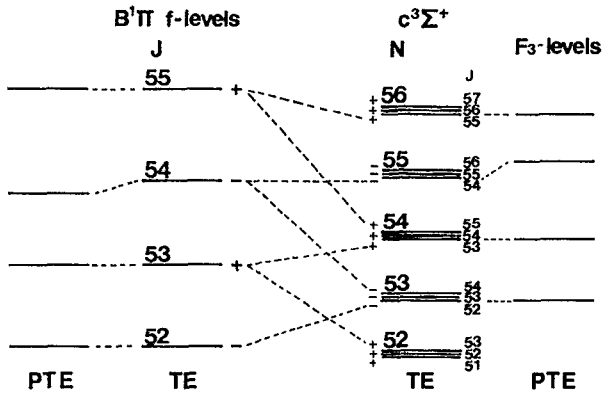

FIG. 3. Perturbing levels of the $B\,^1\Pi(v'=7, J=52\text{–}55\,f)$ and $c\,^3\Sigma^+$ $(v=22, N=52\text{–}56)$ levels. Term energies in the absence of the spin–orbit interaction are expressed as TE and the perturbed term energies are expressed as PTE. The levels, which perturb each other and result in the energy shifts, are connected by a broken line.

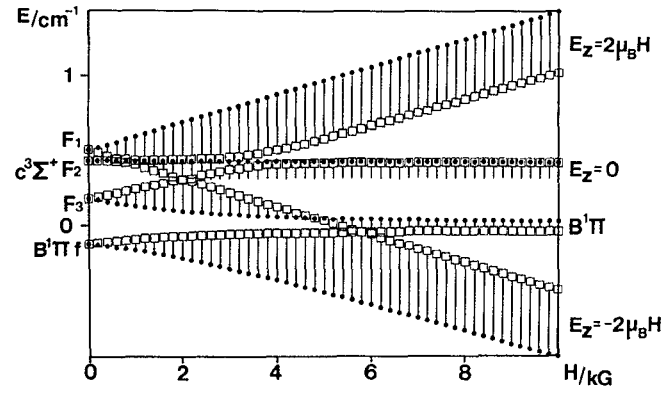

FIG. 4. Calculated energies of the $B\,^1\Pi(v'=7, J=54, M\,f)$, $c\,^3\Sigma^+$ $(v=22, N=55, F_3, M)$, $c\,^3\Sigma^+$ $(v=22, N=55, F_2, M)$, and $c\,^3\Sigma^+$ $(v=22, N=55, F_1, M)$ sublevels are plotted against the magnetic field (plotted at every 200 G). The values for $M=54$ are plotted by filled circles (●). The values for $M=-54$ are plotted by open squares (□). The effects of the hyperfine interaction are not included.

unperturbed and observed energies of the $B\,^1\Pi(v'=7, J=54\,f)$ level, the magnitude of the spin–orbit interaction constant ξ between the $B\,^1\Pi(v'=7, J=54\,f)$ and $c\,^3\Sigma^+$ $(v=22, N=55, J=54)$ levels is determined to be 0.209 cm^{-1}. In this evaluation, we neglected the perturbation between the $B\,^1\Pi(v'=7, J=54\,f)$ and $c\,^3\Sigma^+(v=22, N=53, J=54)$ levels. This is reasonable because the energy spacing between the $B\,^1\Pi(v'=7, J=54\,f)$ and $c\,^3\Sigma^+$ $(v=22, N=53, J=54)$ levels is much larger than the energy of the spin–orbit interaction.

The three levels $|^3\Sigma^+ vN=JJ-1M\rangle$, $|^3\Sigma^+ vN=JJM\rangle$, and $|^3\Sigma^+ vN=JJ+1M\rangle$ split into three separate levels by the spin–rotation interaction H_{SR} and the spin–spin interaction H_{SS}. The nonvanishing matrix elements of $H_{SR}+H_{SS}$ for these wave functions are also given in Ref. 9. The energies of the $B\,^1\Pi(v'=7, J=54\,f)$, $c\,^3\Sigma^+$ $(v=22, N=55, J=54; F_3)$, $c\,^3\Sigma^+(v=22, N=55, J=55; F_2)$, and $c\,^3\Sigma^+(v=22, N=55, J=56; F_1)$ levels are calculated from the spin–spin interaction constant $\lambda_v=0.15$ cm^{-1}, the spin–rotation interaction constant $\gamma_v=0.004$ cm^{-1}, the term energies of the $B\,^1\Pi(v'=7, J=54\,f)$ and $c\,^3\Sigma^+(v=22, N=55, J=54)$ levels,[9] and the spin–orbit coupling constant $\xi=0.209$ cm^{-1}. The results are shown at $H=0$ limit in Fig. 4.

An external magnetic field **H** induces the Zeeman interaction

$$H_Z=-m\cdot H, \tag{6}$$

where m is the magnetic moment of a molecule. By expressing the magnetic moment in terms of spherical tensors,[16] the Hamiltonian of the Zeeman interaction is written as

$$H_Z=-(m_0 D^1_{00}-m_{+1}D^1_{0-1}-m_{-1}D^1_{0+1})H, \tag{7}$$

where $m_0=m_z$, $m_\pm=\mp 2^{-1/2}(m_x\pm im_y)$ in the molecule-fixed coordinates with the z axis along the molecular axis, D^1_{MN} is the rotation matrix, and the magnetic field is along the space-fixed Z axis. The total magnetic moment of electrons is given by

$$m=-\mu_B(\mathbf{L}+g_e\mathbf{S}), \tag{8}$$

where μ_B is the Bohr magneton and g_e is the g value for an electron. We shall neglect the small magnetic moments of nuclei and of molecular rotation. The Zeeman interaction H_Z induces the splittings of energy levels of the $^1\Pi$ and $^3\Sigma^+$ states and the nonvanishing matrix elements are for a $^1\Pi$ state,

$$\langle {}^1\Pi vJM^e_f|H_Z|{}^1\Pi vJM^e_f\rangle=\mu_B H\frac{M}{J(J+1)}, \tag{9}$$

and for a $^3\Sigma^+$ state,

$$\begin{aligned}
\langle {}^3\Sigma^+ vN&=JJ+1M|H_Z|{}^3\Sigma^+ vN=JJ+1M\rangle\\
&=g_e\mu_B HM/(J+1),\\
\langle {}^3\Sigma^+ vN&=JJ+1M|H_Z|{}^3\Sigma^+ vN=JJM\rangle\\
&=g_e\mu_B H\left[\frac{J(J+M+1)(J-M+1)}{(J+1)^2(2J+1)}\right]^{1/2},\\
\langle {}^3\Sigma^+ vN&=JJM|H_Z|{}^3\Sigma^+ vN=JJM\rangle\\
&=g_e\mu_B HM/J(J+1),\\
\langle {}^3\Sigma^+ vN&=JJM|H_Z|{}^3\Sigma^+ vN=JJ-1M\rangle\\
&=g_e\mu_B H\left[\frac{(J+1)(J+M)(J-M)}{J^2(2J+1)}\right]^{1/2},\\
\langle {}^3\Sigma^+ vN&=JJ-1M|H_Z|{}^3\Sigma^+ vN=JJ-1M\rangle\\
&=-g_e\mu_B HM/J.
\end{aligned} \tag{10}$$

The Zeeman interaction has a nonvanishing matrix element only between the same spin states; the selection rule is $\Delta S=0$. Hence, there is no direct Zeeman interaction between the $B\,^1\Pi$ and $c\,^3\Sigma^+$ states.

The level energies in the presence of a magnetic field can be obtained by diagonalizing the matrix of the Hamiltonian $H_0+H_{SO}+H_{SR}+H_{SS}+H_Z$, where H_0 is the Hamiltonian for a rotating diatomic molecule excluding the effect of an electron spin for the basis functions $|B\,^1\Pi v'JM\rangle$, $|c\,^3\Sigma^+ vN=J+1J+2M\rangle$, $|c\,^3\Sigma^+ vN=J+1J+1M\rangle$, and $|c\,^3\Sigma^+ vN=J+1JM\rangle$. The eigenfunctions are expressed by a linear combination of the basis functions

$$C_1|B\,^1\Pi v'JMf\rangle + C_2|c\,^3\Sigma^+ vN=J+1J+2M\rangle + C_3|c\,^3\Sigma^+ vN=J+1J+1M\rangle + C_4|c\,^3\Sigma^+ vN=J+1JM\rangle, \quad (11)$$

where C_1, C_2, C_3, and C_4 are constants. The transition probability of an excitation from the $X\,^1\Sigma^+$ state to the level expressed by Eq. (11) is proportional to C_1^2. For $J=54$, we have calculated the level energies and the eigenfunctions for various magnetic field strengths and the level energies are shown schematically in Fig. 4. At high magnetic field, where the Zeeman interaction is much larger than the spin–rotation and spin–spin interactions, the $^3\Sigma^+(vN=JM)$ level splits into three levels $^3\Sigma^+(vN=JME_Z=2\mu_B H)$, $^3\Sigma^+(vN=JME_Z=0)$, and $^3\Sigma^+(vN=JME_Z=-2\mu_B H)$.[14]

Let us now consider the effect of hyperfine interaction. The hyperfine structure composed of four lines are observed both in the Q 54 and ^RQ 54 lines. The hyperfine structure was shown to be caused by the Fermi contact interaction of the Na nuclear spin ($I=3/2$) in the $c\,^3\Sigma^+$ state.[8,9] The matrix elements are obtained by the coupled basis of the total angular momentum $\mathbf{F}=\mathbf{J}+\mathbf{I}_1$, where $\mathbf{J}$ is the total angular momentum excluding nuclear spin and $\mathbf{I}_1$ is the nuclear spin angular momentum of nucleus 1. The nonvanishing matrix elements of the Fermi contact interaction for the $^3\Sigma^+$ levels are[8,17]

$$\langle c\,^3\Sigma^+ vN=J+1JMI_1FM_F| H_{FC}|c\,^3\Sigma^+ vN=J+1JMI_1FM_F\rangle = A\{[2J(J+1)]^{-1/2}[J/(2J+1)] - [2J(J+1)]^{1/2}/(2J+1)\},$$

$$\langle c\,^3\Sigma^+ vN=JJMI_1FM_F|H_{FC}|c\,^3\Sigma^+ vN=JJMI_1FM_F\rangle = A[2J(J+1)]^{-1/2},$$

$$\langle c\,^3\Sigma^+ vN=J-1JMI_1FM_F| H_{FC}|c\,^3\Sigma^+ vN=J-1JMI_1FM_F\rangle = A\{[2J(J+1)]^{-1/2}[(J+1)/(2J+1)] + [2J(J+1)]^{1/2}/(2J+1)\}, \quad (12)$$

where

$$A=[F(F+1)-J(J+1)-I_1(I_1+1)]\times[4J(J+1)]^{-1/2}K(1;0v1;0v1) \quad (13)$$

and

$$K(1;0v1;0v1)=(8\pi/3)\zeta(1)\langle 0v1\,||\sum_i S_1(i)\delta(r_{i1})||0v1\rangle\,. \quad (14)$$

We determined the $K(1;0v1;0v1)$ value to be 0.0147 cm^{-1} for the $c\,^3\Sigma^+(v=22)$ level by analyzing the magnitude of the hyperfine splitting at $H=0$.

By diagonalizing the matrix of $H_0+H_{SO}+H_{SR}+H_{SS}+H_Z+H_{FC}$, we obtained the level energies and the eigenfunctions. Once the eigenfunctions are obtained, we can calculate the intensity of the polarization spectrum. The Doppler width of NaK at 550 K is about 0.05 cm^{-1} and the Zeeman splitting between the FM_F and $FM_F\pm1$ sublevels is smaller than the Doppler width at $H<10$ kG. The intensity of the transition to the Zeeman sublevel of each F is proportional to C_1^4 multiplied by Eq. (4), of which J and M are replaced, respectively, by F and M_F. By assuming the Lorentzian line shape and the linewidth [full width at half-maximum (FWHM)] of 40 MHz, we plotted the relative intensities against the transition energies for $H=0$, 1.2, and 1.8 kG. The results are shown in Fig. 5. The calculated spectra are in good coincidence with the observed spectra (Fig. 2).

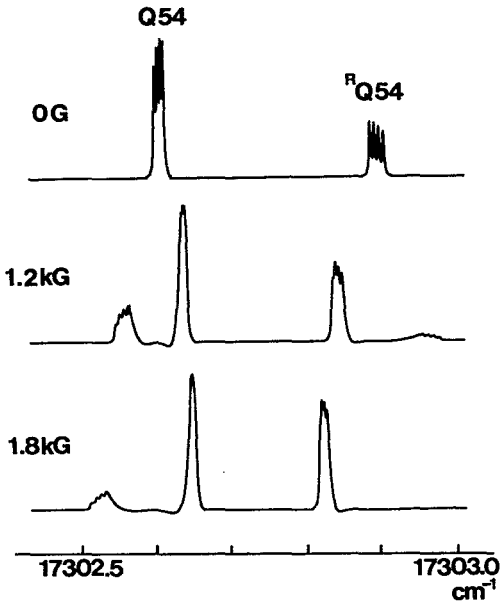

FIG. 5. Calculated intensities are plotted against the transition energies for the $Q\,54\,B\,^1\Pi(v'=7, J=54f)$–$X\,^1\Sigma^+(v''=0, J=54)$ and $^RQ\,54\,c\,^3\Sigma^+(v=22, N=55, F_3)$–$X\,^1\Sigma^+(v''=0, J=54)$ transitions for $H=0$, 1.2, and 1.8 kG. All transition lines are assumed as the Lorentzian curve of FWHM = 40 MHz.

In the weak magnetic fields, each of the four peaks of the Q 54 and ^RQ 54 lines is observed to split into two peaks (see Fig. 6). This is due to the Zeeman splitting of each hyperfine component. In the Q line, the intensity has maxima at $M_F=\pm F$. Hence, each F component splits and shows two maxima at $M_F=F$ and $M_F=-F$. In the strong field, the angular momenta $\mathbf{I}_1$ and $\mathbf{J}$ strongly couple with the magnetic field and F is no longer a good quantum number.[18] The hyperfine splitting, which is about 0.02 cm^{-1} for the ^RQ 54 line, becomes negligible as the magnetic field increases. Calculated energies of the Zeeman sublevels are plotted against H in Fig. 4. The pattern of the Zeeman splitting approaches at $H>5$ kG to the one in the strong field limit.

The Zeeman splitting of a $^1\Pi(vJ)$ level, which is given by Eq. (9), is appreciable for low J levels, but small for high J levels; the Zeeman splitting at 1 kG is calculated to be 0.016 cm^{-1} for $J=5$ and 0.002 cm^{-1} for $J=50$. Therefore, the observed large Zeeman splitting of the $B\,^1\Pi(v'=7, J=54)$ level is due to strong mixing with the $c\,^3\Sigma^+(v=22, N=55, J=54; F_3)$ level. As we can see from Eq. (10), the $c\,^3\Sigma^+(v=22, N=55, F_3, M>0)$ sublevels shift toward low energy and the $c\,^3\Sigma^+(v=22, N=55, F_3, M<0)$ sublevels shift toward high energy. If the spin–orbit interaction is neglected, the level crossing between the $B\,^1\Pi(v'=7, J=54,$

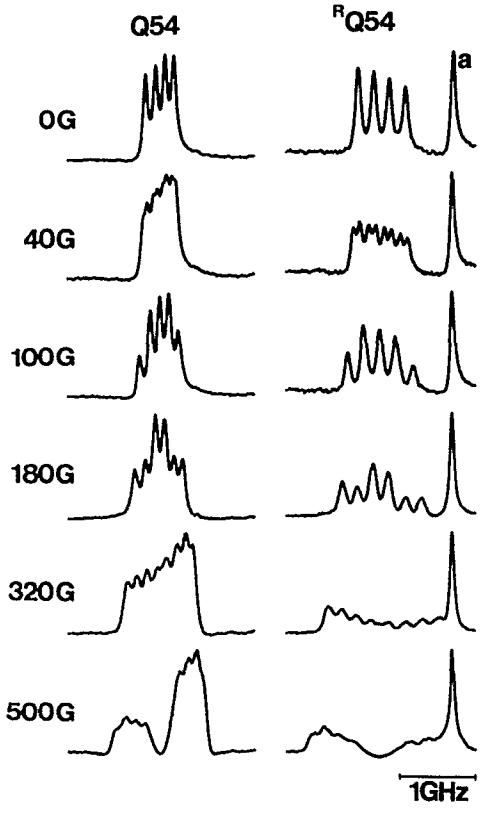

FIG. 6. Doppler-free polarization spectra for the $Q\,54\ B\,^1\Pi(v'=7, J=54\ f)$–$X\,^1\Sigma^+(v''=0, J=54)$ and $^RQ\,54\ c\,^3\Sigma^+(v=22, N=55, F_3)$–$X\,^1\Sigma^+(v''=0, J=54)$ transitions in weak magnetic fields. a is the line of the $B\,^1\Pi(v'=8, J=68\ e)$–$X\,^1\Sigma^+(v''=0, J=67)$ transition.

$M>0$) and $c\,^3\Sigma^+$ ($v=22, N=55, F_3, M>0$) sublevels occurs at about 1–2 kG depending on M. The spin–orbit interaction occurs between the same M levels as we can see from Eq. (5). The smaller the energy separation between the perturbing levels, the larger are their shifts. As the magnetic field increases to about 2 kG, the $c\,^3\Sigma^+$ ($v=22, N=55, F_3, M>0$) sublevels increase the character of $B\,^1\Pi$ and the $B\,^1\Pi$ ($v'=7, J=54, M>0$) sublevels increase the character of $c\,^3\Sigma^+$ ($v=22, N=55, F_3$). On the other hand, the $c\,^3\Sigma^+$ ($v=22, N=55, F_3, M<0$) sublevels increase the character of $c\,^3\Sigma^+$ and the $B\,^1\Pi(v'=7, J=54, M<0)$ sublevels increase the character of $B\,^1\Pi$. These facts appear on the Zeeman spectra as the changes in the intensity and line shape (see Figs. 2, 4, and 5).

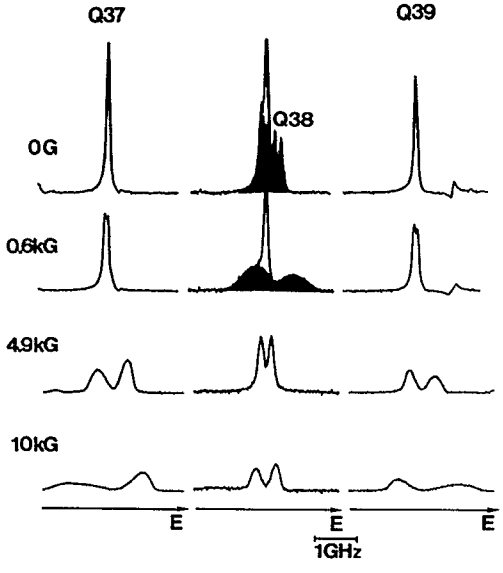

FIG. 7. Doppler-free polarization spectra for the $Q\,37$, $Q\,38$, and $Q\,39$ lines of the $B\,^1\Pi(v'=9)$–$X\,^1\Sigma^+(v''=0)$ transition and the changes with the external magnetic field. The $Q\,38$ line, which is shaded, is broadened out in the strong magnetic field and the residual is an overlapped line of the $B\,^1\Pi(v'=12, J=41\ f)$–$X\,^1\Sigma^+(v''=1, J=41)$ transition.

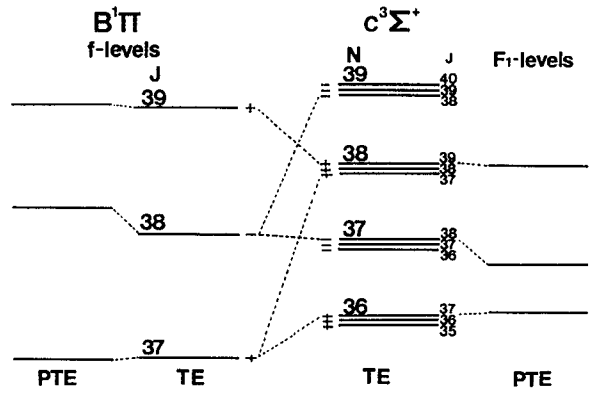

FIG. 8. Perturbing levels of the $B\,^1\Pi(v'=9, J=37\text{–}39\ f)$ and $c\,^3\Sigma^+$ ($v=24, N=36\text{–}39$) levels. Term energies in the absence of the spin–orbit interaction are expressed as TE and the perturbed term energies are expressed as PTE. The levels, which perturb each other and result in the energy shifts, are connected by a broken line.

The line shapes of the $Q\,37$, $Q\,38$, and $Q\,39$ lines of the $B\,^1\Pi(v'=9)$–$X\,^1\Sigma^+(v''=0)$ transitions are found to change differently as the external magnetic field increases (see Fig. 7). The term energies (TE) in the absence of the spin–orbit interaction and the perturbed term energies (PTE) of the $B\,^1\Pi(v'=9, J=37\text{–}39)$ and $c\,^3\Sigma^+(v=24, N=36\text{–}39)$ levels at zero field are shown schematically in Fig. 8. Large Zeeman splitting of the $Q\,38$ line is a result of the strong perturbation with the $c\,^3\Sigma^+(v=24, N=37, J=38)$ level. The line shapes of the Zeeman spectra of the $Q\,37$ and $Q\,39$ lines are asymmetric. The magnitude of the perturbation is different between the magnetic sublevels. The Zeeman spectra of the transitions to the $B\,^1\Pi(v'=9, J=37, M<0)$ sublevels (low energy side) are observed with larger shift and weaker intensity than those of the $B\,^1\Pi(v'=9, J=37, M>0)$ sublevels. This is due to the fact that perturbing $c\,^3\Sigma^+(v=24, N=36, J=37)$ level is located at higher energy than the $B\,^1\Pi(v'=9, J=37)$ level. On the other hand, the Zeeman spectrum of the transitions to the $B\,^1\Pi(v'=9, J=39, M>0)$ sublevels (high energy side) is observed with larger shift and weaker intensity than the one to the $B\,^1\Pi(v'=9, J=39, M<0)$ sublevels. Strongly perturbed levels are observed with large shift and small intensity, which is the result of strong mixing of the $c\,^3\Sigma^+$ level. From the change of the line shape by the magnetic field, we can know whether the interacting level is located on the high or low energy side. The pattern of the Zeeman spectrum is useful to get an additional information on the perturbing state.

ACKNOWLEDGMENTS

The authors thank Mr. K. Yokoyama for his help at an early stage of this work. This work is partly supported by a Grant-in-Aid for scientific research from the Ministry of Education, Science, and Culture of Japan.

[1] M. S. Sorem, Ph. D. thesis, Stanford University, 1972.
[2] W. H. Jeng, X. Xie, L. P. Gold, and R. A. Bernheim, J. Chem. Phys. **94**, 928 (1991).
[3] R. F. Barrow, R. M. Clements, J. Derouard, N. Sadeghi, C. Effantin, J. d'Incan, and A. J. Ross, Can. J. Phys. **65**, 1154 (1987).
[4] P. Kowalczyk, B. Krüger, and F. Engelke, Chem. Phys. Lett. **147**, 301 (1988).
[5] J. Derouard and N. Sadeghi, J. Chem. Phys. **88**, 2891 (1988).
[6] M. Baba, S. Tanaka, and H. Katô, J. Chem. Phys. **89**, 7049 (1988).
[7] J. Derouard, H. Debontride, T. D. Nguyen, and N. Sadeghi, J. Chem. Phys. **90**, 5936 (1989).
[8] P. Kowalczyk, J. Chem. Phys. **91**, 2779 (1989).
[9] H. Katô, M. Sakano, N. Yoshie, M. Baba, and K. Ishikawa, J. Chem. Phys. **93**, 2228 (1990).
[10] C. Wieman and T. W. Hänsch, Phys. Rev. Lett. **36**, 1170 (1976).
[11] R. E. Teets, F. V. Kowalski, W. T. Hill, N. Carlson, and T. W. Hänsch, SPIE **113**, 80 (1977).
[12] M. Raab, G. Höning, W. Demtröder, and C. R. Vidal, J. Chem. Phys. **76**, 4370 (1982).
[13] H. Katô, T. Kobayashi, M. Chosa, T. Nakahori, T. Iida, S. Kasahara, and M. Baba, J. Chem. Phys. **94**, 2600 (1991).
[14] H. Katô, M. Baba, and I. Hanazaki, J. Chem. Phys. **80**, 3936 (1984).
[15] A. J. Ross, C. Effantin, J. d'Incan, and R. F. Barrow, Mol. Phys. **56**, 903 (1985).
[16] D. M. Brink and G. R. Satchler, *Angular Momentum* (Oxford University, Oxford, 1968).
[17] The sign of the second term of $\langle {}^3\Sigma^+ vN = J \pm 1 J M I_1 F_1 M_{F_1} | H_{FC}(1) | {}^3\Sigma^+ vN = J \pm 1 J M I_1 F_1 M_{F_1} \rangle$ in Ref. 9 should be changed as Eq. (12) in this article.
[18] C. H. Townes and A. L. Schawlow, *Microwave Spectroscopy* (McGraw–Hill, New York, 1955).